

## Coastal Water Properties and Hydrodynamic Processes in the Malacca Strait: Case Study Northeastern Coast of Sumatra, Indonesia

Alan Frendy Koropitan<sup>1\*</sup>, Ternala Alexander Barus<sup>2</sup>, Muhammad Reza Cordova<sup>3,4</sup>

<sup>1</sup> Department of Marine Science and Technology, Faculty of Fisheries and Marine Science, IPB University, Jl. Agatis, Dramaga, Bogor, 16680, Indonesia

<sup>2</sup> Department of Biology, Faculty of Mathematic and Natural Sciences, University of Sumatera Utara, Jl. Abdul Hakim No.1, Medan, 20155, Indonesia

<sup>3</sup> Research Center for Oceanography, Indonesian Institute of Sciences, Jl. Pasir Putih 1, Jakarta Utara, DKI Jakarta, 14430, Indonesia

<sup>4</sup> Research Center for Oceanography, Earth Sciences Research Organization, National Research and Innovation Agency, Jl. Pasir Putih 1, Jakarta Utara, DKI Jakarta, 14430, Indonesia

\* Corresponding author's e-mail: alan@apps.ipb.ac.id

### ABSTRACT

Dynamic processes in the coastal waters play an important role in regulating the marine pollution distribution caused by riverine inputs and are relevant for coastal management. Here, the coastal water properties were investigated from field measurements and modeling hydrodynamic processes in the northeastern coast of Sumatra. The present study found that the river discharges affect a low salinity of 28–29 psu in the surface waters along near the coastal line. The river discharge might influence by strong La Niña with high rainfall in December 2010. However, the authors suggested that the effect of tidal mixing is stronger than the freshwater discharges, resulting in vertically well-mixed coastal waters in the region. The observed tidal range of 200 cm indicates a strong tidal mixing in the waters. The tidal elevation contributes more than 70% of the total measured sea elevation. The tidal current signal in which the flow pattern simulations show no significant differences among tide and wind-tide driven currents, is also dominant (77%).

**Keywords:** vertically well-mixed, tidal mixing, coastal pollution, flow pattern

### INTRODUCTION

The Malacca Strait is one of the major international seaways. With high traffic density (Rusli 2012), this strait links the Indian Ocean to the Andaman Sea in the North and the South China Sea in the South. The wide section and depth of the Northern Malacca Strait are gradually declining and narrowing down to the Southern Strait (Muhaimin A et al. 2011). Malacca Strait is a part of the Sunda Shelf, shallow water (Minhat et al. 2020), and included in the mainland of Asia as well as some waters and bays such as the South China Sea, Gulf of Thailand, and the Java Sea. The southern, narrowest, part of Malacca Strait is about 30 m deep and 35 km wide. The depth

increases gradually to about 100 m before the continental slope to the Andaman Sea begins (Devlin et al. 2018; Wyrcki 1961). On the bottom of this strait, in which strong tidal currents occur, large sand ripples of considerable uniformity are formed, with crests perpendicular to the direction of the tidal currents (Wyrcki 1961).

The Malacca Strait is significantly influenced by flow pattern and hydrographic parameters. The Malacca Strait is typically viewed as a normal, wind-driven channel with other components considered negligible (Chen et al. 2014). This shallow strait includes unique ecosystems of muddy bottom sediments and hyposalinic waters (Thia-Eng et al. 2000). The Strait of Malacca has a tropical atmosphere, with monsoon winds reversing twice

a year (Tan et al. 2006). The two main monsoon seasons are the wet Northeast Monsoon and the warm and dry season of the Southwest Monsoon. During the Southwest Monsoon, the intrusion of the Andaman Sea from the Northern part of the Malacca Strait happened (Daryabor et al. 2016; Ibrahim and Yanagi 2006; Tomczak and Godfrey 1994). During the Northeast Monsoon, the water from the South China Sea penetrated at least the Southern portion (Pang and Tkalich 2003). The tidal current is strengthened in the northern Malacca Strait, while the southern strait narrow channel is reduced. The winds with high intensity and wind-stress curl may create an eddy as wide as the width of the northern channel, which significantly distorts the tidal circulation, particularly during the neap tide (Chen et al. 2014). The motions of these water intrusions affect the physical properties, such as dissolved oxygen, water temperature, and salinity (Daryabor et al. 2016; Ibrahim and Yanagi 2006).

The strong hydrodynamic processes in the Malacca Strait are more complicated due to river discharge from Sumatra and Peninsular Malaysia as well as the structure and incident waves in this area (Chua et al. 1997; Hii et al. 2006; Jaya et al. 1998; Pang and Tkalich 2003). Sea Surface Temperature (SST) and Sea Surface Salinity (SSS) are the most important oceanographic variables. SST variability in Malacca Strait is determined by heat and water balance, ocean morphology, bathymetry, and meteorological factors such as rainfall, evaporation, air temperature, wind speed, and sunlight (Aldrian and Dwi Susanto 2003; Chen et al. 2014; Deser et al. 2010; Fingas 2018). SSS is affected by evaporation and rainfall (Corrège 2006; Durack and Wijffels 2010; Muhaimin A et al. 2011). Higher evaporation contributes to greater SSS values. On the other side, higher evaporation contributes to lower SSS. Thus, hydrodynamic processes, sea temperature and salinity can be used to examine the oceanographic and climatic conditions in the Malacca Strait.

The Malacca strait has potentially a large number of natural resources (Sangkoyo et al. 2011; Thia-Eng et al. 2000), such as oil and gas and fishery. In the Indonesian part, the Malacca Strait stretches along the northeastern coast of Sumatra; Aceh, North Sumatra, and Riau Provinces (Sangkoyo et al. 2011). The rapid rise in anthropogenic activities in the Malacca Strait could be leading to the degradation of marine habitats and indirectly deteriorating ecosystem services (Islam

and Maznah 2018), including seawater physical properties.

It is, therefore, crucial to examine the oceanographic and climatic conditions in the Malacca Strait, especially in the direct adjacent region of Indonesia (northeastern coast Sumatra), where studies are still little done. Knowing temperature, salinity, and hydrodynamic processes is vital to oversee the management of this strait, particularly for the Indonesian government, and to manage the marine environment in eastern Sumatra. The primary aim of this paper was to investigate the physical properties pattern of water masses from field measurements of seawater temperature, salinity and modeling hydrodynamic processes in the northeastern coast of the Sumatra region, adjacent to the Malacca Strait.

## THE MATERIAL AND METHOD

### Study Area

Field observation was conducted along the east coast of North Sumatra Province, which is Deli Serdang Regency, Medan City, and Langkat Regency, including some regions of Aceh Province covering Aceh Tamiang Regency and Langsa City. This area is the northwest boundary of the Malacca Strait. The northwest border is set in a gentle bottom slope, avoiding the steep slope between the Andaman Sea and the Malacca Strait (Chen et al. 2014). This makes it interesting to study this area.

### Field Sampling

The CTD (Conductivity Temperature and Depth) was used at multiple stations to measure the seawater temperatures and salinity at all water depths. The CTD was guided down to the water, where the collected results were calculated for an interval of 0.1 m. During coastal water measurements, the authors used Arcturus Navigation Vessel for 3-day cruising (7–9 December 2010), and collected temperature and salinity from 56 stations in six transects along Belawan to Langsa, which cover six transecting lines from the coast (Figure 1). A one-day cruise boat (12 December 2010) was used to cover nine stations near the coastline of Belawan until Pangkalan Susu, in particular to conduct the CTD measurements in coastal waters (Figure 1).

Water depth was measured by using Garmin GPSMap Sounder 421s with distance interval recording around 10 m. The sounder was attached in the Navigation Vessel of Arcturus to measure the water depth in coastal waters following the vessel tracking and vessel speed of 5–6 knots. The total transect length in coastal waters is 120 nm (nautical mile). For the water depth measurement in coastal waters, the sounder was attached in the boat, which moved at the same speed as the Navigation vessel, with a total transect length of 55 nm. The water depth measured by the sounder was then corrected with the mean sea-level obtained from the tidal prediction data in the nearest location (Aru Bay).

Elevation of sea level and ocean currents were measured by using a tide gauge and current meter, respectively. The tide gauge was deployed in the local harbor, while the current meter was deployed further of the coastal to avoid non-linear signals that might affect the recorded water current. The non-linear effect could be caused by

wave reflection near the coastal or produced by a running boat. The hourly sea level elevation measurement was recorded for 699 hours, while the hourly ocean current measurement was recorded for 704 hours. The specific location of the tide gauge and current meter deployments is presented in Figure 1.

#### Time series analysis for sea-level elevation and ocean current data

The sea level elevation was analyzed using the least-squares method in MATLAB, referred to as the *t\_tide* program (Pawlowicz et al. 2002). This program is similar to the FORTRAN code described by previous research (Foreman 1977, 1978; Godin 1972). However, unlike those authors, the *t\_tide* program directly uses complex algebra, rather than dealing with sine and cosine separately. The analysis includes as many as 146 possible tidal constituents, 45 of them being astronomical in origin, while the remaining 101 are shallow-water constituents. Similar to sea level,

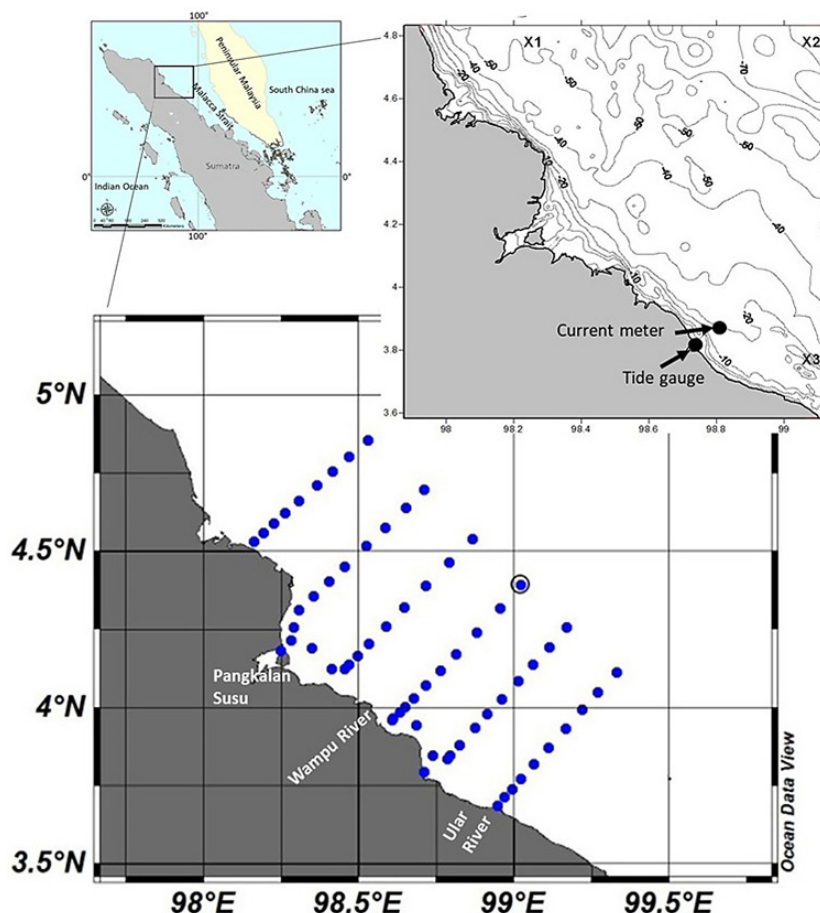


**Fig. 1.** Location of CTD measurements (blue dots), bathymetric profile of the model region, location of tide gauge and current meter (black dots) and geographic positions of predicted tidal constituents of ORI.96 for tidal elevation along open boundary, X1 (4.75 N and 98.25 E), X2 (4.75 N and 99.25 E) and X3 (3.75 N and 99.25 E).

the analysis of the ocean current data were also conducted using the least-squares method of the `t_tide` program (Pawlowicz et al. 2002).

The type of tides in the site observation was determined quantitatively according to the *Formzahl* number, which is calculated from the tidal amplitude ratio between diurnal and semi-diurnal constituents. The *Formzahl* number is as follow:

$$F = \frac{O_1 + K_1}{M_2 + S_2}$$

where:  $F$  – *Formzahl* number

$O_1$  – tidal amplitude of the diurnal constituent forced by the Moon,

$K_1$  – tidal amplitude of the diurnal constituent forced by the Moon and the Sun,

$M_2$  – tidal amplitude of the semi-diurnal constituent forced by the Moon,

$S_2$  – tidal amplitude of the semi-diurnal constituent forced by the Sun.

On the basis of  $F$ , the type of tides is classified into;

- $F < 0.25$  – semi-diurnal tide,
- $0.26 < F < 1.50$  – mixed tide pre-dominantly semi-diurnal,
- $1.51 < F < 3.00$  – mixed tide pre-dominantly diurnal,
- $F > 3.00$  – diurnal tide.

### Hydrodynamic Model

The developed hydrodynamic model is based on the Princeton Ocean Model (POM) with depth-averaged approximation (two-dimensional/2-D) (Blumberg et al. 1999; Blumberg and Mellor 1987). POM provides a 3-D model for fixed density and baroclinic and performs time splitting mode to reduce the computation time. Time splitting is a numerical technique to separate gravitation wave calculation in the complete 3-D model equation (Zhang et al. 2004). That means the gravitation wave propagation in the surface water can be calculated well using a 2-D model equation, while the internal gravitation wave, which moves slower than the surface wave, can be simulated in a 3D model equation with a longer time step (Blumberg and Mellor 1987). Therefore, the time splitting mode has two-timed steps; a short time step (external mode) for the 2-D model and a long-time step (internal mode) for a 3-D model. POM uses a sigma coordinate for a vertical layer, which allows the model calculation to follow the bathymetry profile (Blumberg and Mellor 1987).

The hydrodynamic model integrated vertically from the bottom ( $\sigma=-1$ ) to the surface water ( $\sigma=0$ ) within the coordinate of sigma. POM uses an incompressible assumption of fluid (Blumberg and Mellor 1987). Since, according to Ekman’s theory, the wind significantly affects the ocean to about 100 m, the hydrodynamic model treated the waters in the study area as a homogenous layer (Zhang et al. 2004). For this reason, in the present study, the external mode was used for water current measuring depth average. Mode external equations of POM are as follows (Mellor 2002):

$$\frac{\partial \eta}{\partial t} + \frac{\partial \bar{U}D}{\partial x} + \frac{\partial \bar{V}D}{\partial y} = 0 \quad (1)$$

$$\begin{aligned} \frac{\partial \bar{U}D}{\partial t} + \frac{\partial \bar{U}^2 D}{\partial x} + \frac{\partial \bar{U}\bar{V}D}{\partial y} - \tilde{F}_x - f\bar{V}D + gD \frac{\partial \eta}{\partial x} = -\langle wu(0) \rangle + \langle wu(-1) \rangle \\ \frac{\partial \bar{V}D}{\partial t} + \frac{\partial \bar{U}\bar{V}D}{\partial x} + \frac{\partial \bar{V}^2 D}{\partial y} - \tilde{F}_y + f\bar{U}D + gD \frac{\partial \eta}{\partial x} = -\langle wv(0) \rangle + \langle wv(-1) \rangle \end{aligned} \quad (2)$$

Equation (1) is a continuity equation and equation (2) is a momentum equation,

where:  $D = H + \eta$

$\bar{U}, \bar{V}$  are depth-averaged velocity components for x-axis and y-axis, respectively with

$$\bar{U} = \frac{1}{D} \int_{-1}^0 U d\sigma \quad (3)$$

$$\bar{V} = \frac{1}{D} \int_{-1}^0 V d\sigma \quad (4)$$

where:  $t$  – time,

$H$  – water depth,

$\eta$  – sea level,

$g$  – gravitation,

$f$  – Coriolis force.

Diffusivity terms:

$$\begin{aligned} \tilde{F}_x = \frac{\partial}{\partial x} \left[ H2\bar{A}_M \frac{\partial \bar{U}}{\partial x} \right] + \frac{\partial}{\partial y} \left[ H\bar{A}_M \left( \frac{\partial \bar{U}}{\partial y} + \frac{\partial \bar{V}}{\partial x} \right) \right] \\ \tilde{F}_y = \frac{\partial}{\partial y} \left[ H2\bar{A}_M \frac{\partial \bar{V}}{\partial y} \right] + \frac{\partial}{\partial x} \left[ H\bar{A}_M \left( \frac{\partial \bar{U}}{\partial y} + \frac{\partial \bar{V}}{\partial x} \right) \right] \end{aligned} \quad (5)$$

where: horizontal diffusivity coefficient  $A_M$  was set to be constant ( $A_M = 100 \text{ m}^2/\text{sec}$ ).

Wind stress over the surface is as follows (Ramming and Kowalik 1980):

$$\begin{aligned} \langle wu(0) \rangle &= \frac{\rho_a C_D wu \sqrt{wu^2 + wv^2}}{D} \\ \langle wv(0) \rangle &= \frac{\rho_a C_D wv \sqrt{wu^2 + wv^2}}{D} \end{aligned} \quad (6)$$

where:  $\rho_a$  and  $C_d$  are air density and drag coefficient in the surface, respectively, while  $wu$  and  $wv$  are wind velocity component in x-axis and y-axis, respectively. For the bottom shear stress, POM uses quadratic law, as follows (Ramming and Kowalik 1980):

$$\begin{aligned} \langle wu(-1) \rangle &= \frac{C_z \bar{U} \sqrt{\bar{U}^2 + \bar{V}^2}}{D} \\ \langle wv(-1) \rangle &= \frac{C_z \bar{V} \sqrt{\bar{U}^2 + \bar{V}^2}}{D} \end{aligned} \quad (7)$$

where:  $C_z$  (0.0025) is a bottom shear constant.

The model region has 137 by 139 grid points with grid sizes ( $dx$  and  $dy$ ) of 1 km. According to Courant-Friedrichs-Lewy (CFL) criteria for numerical stability, then the external time step ( $dt_E$ ) was set to be 5 seconds where the equation (Mellor 2002) is:

$$dt_E \leq \frac{1}{2\sqrt{gH} + V_{max}} \sqrt{\frac{1}{dx^2} + \frac{1}{dy^2}} \quad (8)$$

where:  $V_{max}$  – predicted maximum velocity.

Boundary conditions of the model region are as follows:

- close boundary condition (land)  $(\bar{U}, \bar{V}, \eta) = 0$
- open boundary condition (adjacent water)

The sea level along open boundary was input using the predicted tidal elevation of three main constituents (K1, M2 and S2) obtained from ORI.96 (global tidal model assimilated with satellite Altimetry data of Topex/Poseidon). The model region and positions of predicted tidal elevation along the open boundary are presented in Figure 1, while detailed information of tidal constituents is given in Table 1.

The tidal elevations in between are calculated by linear interpolation. In addition, the water currents along the open boundary are calculated according to the radiation equation (Kowalik and Murty 1993):

$$\frac{\partial \bar{U}}{\partial t} \pm C \frac{\partial \bar{U}}{\partial x} = 0 \quad (9)$$

where:  $C = (gH)^{0.5}$ , which long wave velocity.

#### Model validation

A comparison between the model results and the observed tidal elevation, as produced by the `t_tide` program (Table 2), shows that three main constituents are reliable and consistent, where the amplitude difference is only 5 cm or less. The phase difference between the model result and observed data are still comparable.

Generally, the calculated tidal currents of the `t_tide` program are moderately comparable with the observed data (Table 3). Comparing the model results with observed tidal current reveals that the variations in semi-diurnal components are remarkably higher than diurnal. This result is caused by the topographic effect that is not resolved well in the model region. The 2-dimensional model itself is also not resolved vertical water movement profile, so that the observed current data in specific depth may influence it. However, the model results for inclination is still lower than 45°, which showed that the calculated flow pattern is still comparable with the natural condition.

**Table 1.** Tidal components obtained from ori.96 in the stations of X1, X2 And X3

Tide constituents	X1		X2		X3	
	Amp (cm)	Phase (°GMT)	Amp (cm)	Phase (°GMT)	Amp (cm)	Phase (°GMT)
K1	26.59	225.69	23.9	233.10	27.0	240.44
M2	43.28	187.10	38.20	203.44	44.02	217.93
S2	30.81	206.67	26.80	222.16	31.85	236.26

\*Amp: Amplitude

**Table 2.** Comparison between the model results and observed tidal elevation using a tide gauge

Tidal constituent	Delta amplitude (cm)	Delta Phase (° GMT)
K1	0.93	2.06
M2	5.08	11.25
S2	2.27	25.12

## RESULTS AND DISCUSSIONS

### Temperature and Salinity

The observational data showed that SST in the study area is generally constant (29°C) during December 2010, as shown in Figure 2. The variability of SST in the Indonesian seas is around 26–28°C due to constant light intensity all year round. However, the Indonesian seas are also under a monsoon system, so it relies on a monsoonal wind pattern. In the western area of Indonesia, SST was predominantly lower during December-February than in the eastern part, and in June-August. The distribution by the SST in the Malacca Strait amounts to about 28–30°C during Southwest Monsoon (June – August) and decreases by 1–2°C during Northeast Monsoon (December – February) (Thia-Eng et al. 2000). In general, mean SST along the Malacca Strait varies between 28 and 30°C (Pang and Tkalich 2003; Thia-Eng et al. 2000; Wyrski 1961).

Figure 2 shows the observed SSS in the study area. It presents low salinity that indicates discharge from rivers, with concentrations of 28–29 psu (equivalent to ppt) in Pangkalan Susu Bay and near river mouths. This value is still high for such river mouths. The freshwater has been mixed and might not dominate the study area, as shown by the SSS distribution around 31–31.5 psu. However, the salinity in the strait is lower than 32 ppt during the year (Pang and Tkalich 2003; Thia-Eng et al. 2000; Wyrski 1961), lower than on the east coast of Peninsular Malaysia (>32 ppt) that is influenced by oceanic waters. Many large rivers along the strait (Hii et al. 2006; Jaya et al. 1998) contributes to freshwaters, mineral and organic

substance supplies, thus affect the value of SSS (Corrège 2006).

The vertical structure of coastal water properties is shown in Figures 3 (temperature) and 4 (salinity). In general, the vertical temperature distribution at all transects presents a well-mixed profile with a value of about 28–29.5°C.

The temperature profile in the northern transect might show a slightly vertical stratification. However, a thermocline layer does not form due to a slight gradient of temperature. This homogeneous layer of temperature in the coastal waters is under control by tidal mixing, as reported by Osadchiev et al. (2020), Wu and Wu (2018), Susanto et al. (2019). Figure 4 presents slightly stratified waters due to the interactions between the freshwater discharge and tidal mixing, as shown in the salinity cross-section profile in the region. The middle and southern transects located near the estuaries of the Wampu River and the Ular River show a lower salinity of < 32 psu near the river mouth at 10 and 20 m depth, respectively. The low salinity then distributes towards offshore until 20 km (middle transect) and more than 60 km (southern transect) from the coastline.

Related to climate variability, the freshwater discharge in the study area was also influenced by the La Niña event. NOAA's Climate Prediction Center reported that the Oceanic Niño Index (ONI) started a negative SST anomaly in June 2010 by –0.7°C. The peak was September – December 2010 with a negative SST anomaly of –1.6°C (Climate Prediction Center – ONI, NOAA). Therefore, a strong La Niña event occurred during the field measurements in December 2010. In addition, there was an El Niño event from June 2009 until March 2010. The La Niña event causes rainfall increases over the Indonesian archipelago, while El Niño is associated with prolonging the dry season. In terms of the rainfall in Belawan, Sulbakti (2016) reported that monthly rainfall from June 2009 until March 2010 was around 35–96 mm. The rainfall was then peak in December 2010 by 258 mm. However, the obtained findings suggest the effect of freshwater discharge influenced by the strong La Niña is still

**Table 3.** Comparison between the model results and observed tidal current (ellipse component)

Tidal constituent	Delta major ellipse (m/s)	Delta minor ellipse (m/s)	Delta inclination (degree from east)	Delta phase (° GMT)
K1	0.021	0.013	27.83	36.7
M2	0.174	0.038	40.71	33.98
S2	0.031	0.023	41.88	43.04

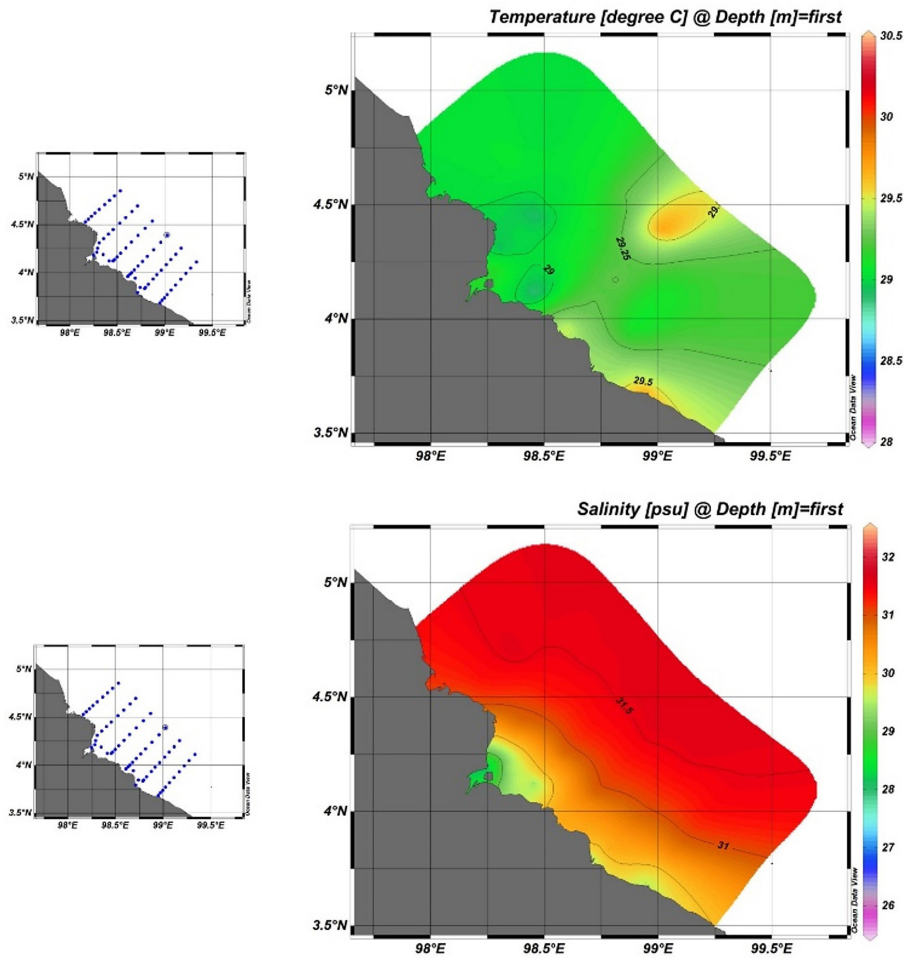


Fig. 2. Sea surface temperature (above) and sea surface salinity (below) distribution in the study area. Practical salinity unit (psu) is equivalent to ppt

lower than the effect of tidal mixing, particularly in controlling the coastal water properties in the study area. The dynamics of tide and tidal current will be discussed in the next sub-chapter.

### Tide and Tidal current

The tides in the Malacca Strait are influenced by tidal propagation from the Indian Ocean that enters the Malacca Strait through the Andaman Sea. Wyrтки (1961) reported that the tidal amplitude increases from 80 cm in the northern part to 250 cm in the southern part, particularly when it approaches the narrowest channel of the Malacca Strait. The bathymetric profile and tidal oscillation cause this. Recently, Haditjar et al. (2020) reported another way of tidal propagation from the South China Sea (SCS). The tides from the Andaman Sea in the north and the tides from the SCS through Singapore Waters in the south of the Malacca Strait meet in the middle, resulting in a shoaling in the region.

Field observation of total sea-level elevation, predicted tidal elevation and residual signal in the region are presented in Figure 5. The tidal range during neap tide is around 100 cm. Meanwhile, in spring, tide could reach more than 200 cm (Figure 5a). The separation between tide (predicted tidal elevation) and non-tide (residual signal) shows that the tide signal is more dominant than the non-tide signal. In this case, the tide signal composition is 72% of the total sea-level elevation. The remained signals or non-tide might be influenced by freshwater discharge, wind and non-linearity effect in the region due to topography profile.

Using the *t\_tide* program for whole possible tidal constituents shows that the K1 (diurnal) and M2, S2 and N2 (Semi-diurnal) components are most dominant (Table 4) for the tidal elevation. Overall, the M2 tide is an essential component of the tidal wave propagation in the region. The *Formzahl* number calculation produces a value of 0.4 so that the tidal type in the study area can

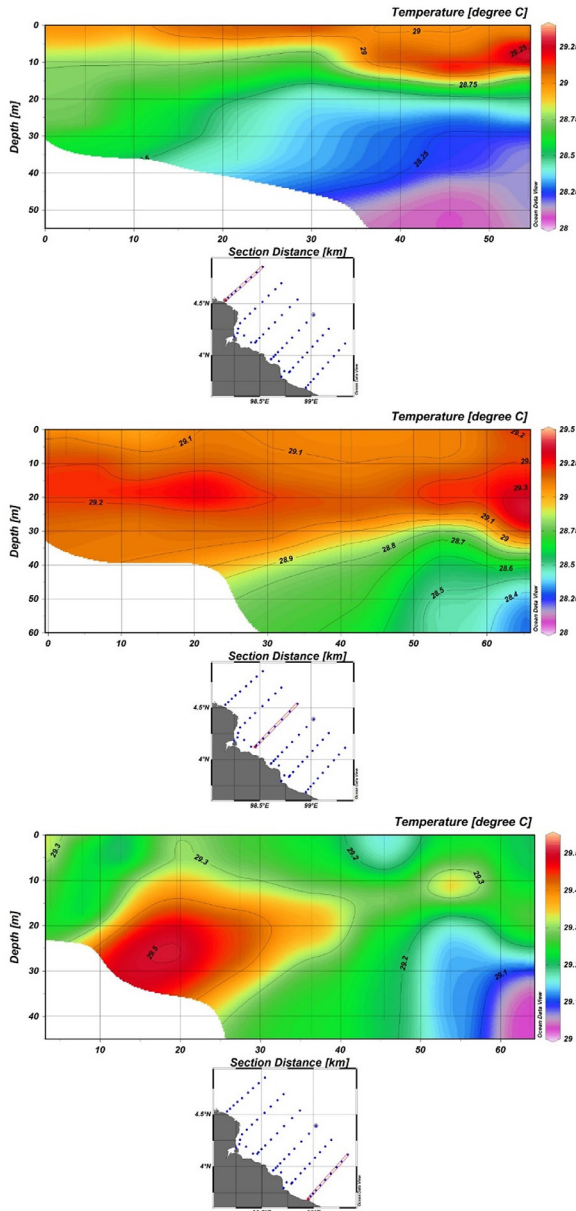


**Fig. 3.** Sea temperature cross-section profile in the northern (above), middle (middle) and southern (below) transects

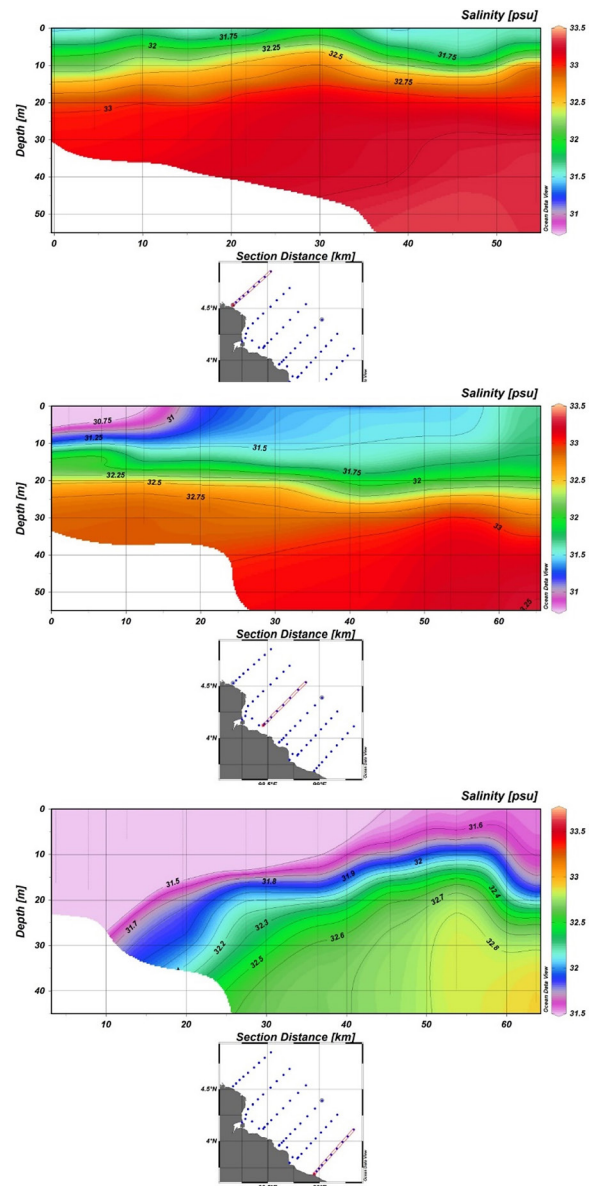


**Fig. 4.** Sea salinity cross-section profile in the northern (above), middle (middle) and southern (below) transects

be categorized as mixed-tide pre-dominantly semi-diurnal.

The analysis of the ocean current signal using *t\_tide* shows that the composition of the tidal current signal is 77% of the total recorded data, meaning that the tidal current is dominant in the region. Particularly for the *u*-velocity component (east-west movement) and *v*-velocity component (north-south movement), the composition of the tidal signal for *u*-component and *v*-component is 33.2% and 82.9%, respectively. The major velocity flow of the *v*-component in the study area is consistent with the tidal propagation from the northwest (Andaman Sea) that enters the Malacca

Strait towards the southeast. The observed current magnitude in the study area varies between 0–0.5 m/s. In detail, the tidal current analysis using *t\_tide* is shown in Table 5. K1, M2, S2 and N2 are major components for the total recorded tidal current signal (Table 5). Similar to tidal elevation, the M2 tidal current is an essential component in the region in general with major ellipse of 0.256 m/s.

Besides the major tidal constituents, Table 4 and Table 5 show the nonlinear tidal constituents that arise from the advective terms, where the complex topography in the study area might influence the variation and friction. The dominant

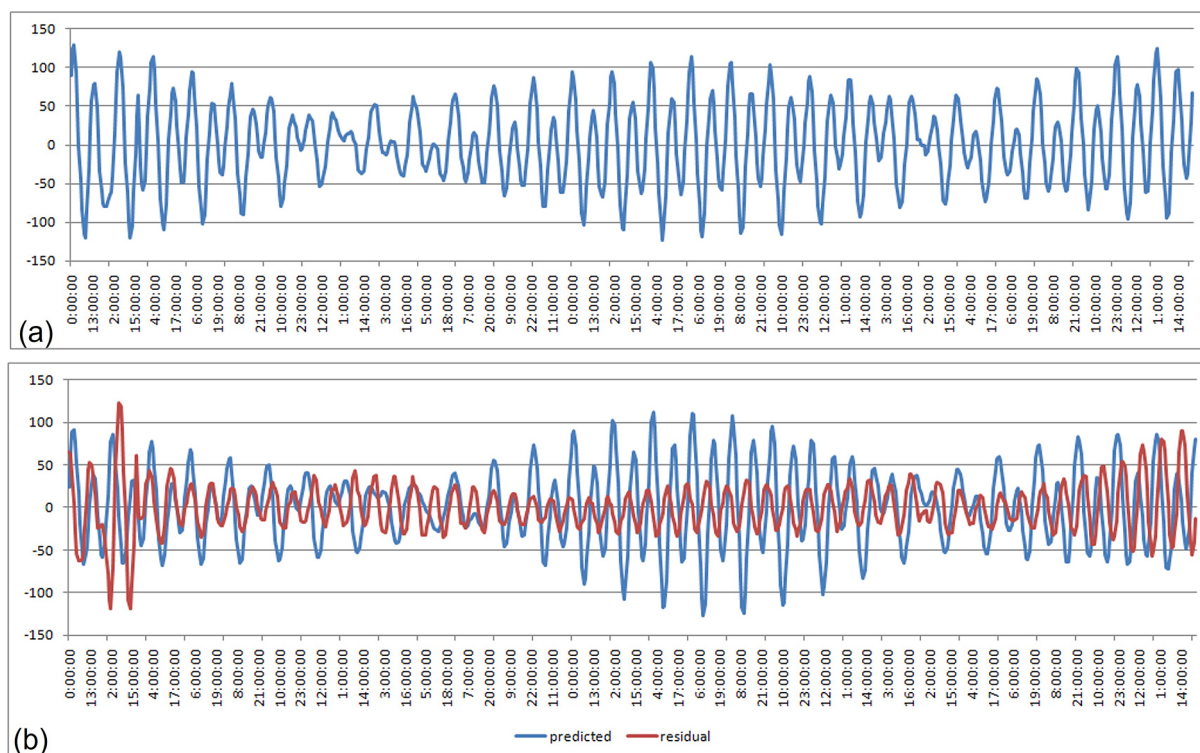


**Figure 5.** Total sea level elevation as recorded by tide gauge (a), predicted tidal elevation and residual signals of the total sea level elevation (b)

tidal constituent of M2 in the study area might produce overtides of M4, M6 and M8, as shown in tidal elevation (Table 4) and tidal current constituents (Table 5).

### Simulated flow pattern

The general flow pattern in the study area is essential in examining the material transport in the waters. The flow patterns assumed that the vertical current profile is similar from the surface until the bottom layers. This condition could be applied for the shallow water with a homogenous (mixed) layer. Therefore, the freshwater effect on water density (vertical and horizontal) is not considered in the model calculation.

According to the observed wind data in Belawan Marine Meteorological Station during period of 1999–2008, the wind was mainly coming from the northeast (81.8%) and a magnitude of 4.76 knots (2.44 m/s). It is followed by west wind (9.15) with a magnitude of 3.86 knots (1.98 m/s), east wind (4.5%) with a magnitude of 4.64 knots (2.38 m/s) and north wind (3.5%) with a magnitude of 4.02 knots (2.06 m/s). The flow patterns were simulated for two different scenarios: tide-driven current (TDC) and wind and tide-driven current (WTDC). Therefore,

three main winds force hydrodynamic model design of WTDC in the study area: northeast (WTDC-NE), west (WTDC-W), and east winds (WTDC-E).

The model results for all scenarios are presented in Figures 6–9. The tidal current patterns during flood spring tide and flood neap tide are pretty similar where the current move from the north and northeast toward the coastline, but the current magnitude during spring is higher than neap tides. A similar pattern is also found during ebb spring and neap tides, but the water moves toward offshore (Figure 6).

The calculated flow pattern for all scenarios shows intensification around Pangkalan Susu Bay caused by a narrow channel around the small island in front of the bay. The influence of wind-driven (Figure 7–9) has appeared during neap tide that the tidal range is minimum.

Considering the depth-averaged model approach of this model, the wind affects the flow pattern, but has little effect on the current magnitude. Therefore, the flow pattern tends to fix when the wind direction is consistent with the flow pattern during ebb or flood tidal current, or reversely, the flow pattern tends to change when the wind direction is opposite or different with the flow pattern during ebb or flood tidal current. In

**Table 4.** List of tidal constituents as recorded by tide gauge

Tide constituent	Amplitude (cm)	Phase (° GMT)
MSF	1.5547	162.26
2Q1	1.0754	350
Q1	1.0777	80.2
O1	3.0153	131.13
NO1	5.0936	276.7
K1	26.5929	232.29
J1	5.5518	338.29
OO1	2.3184	59.59
UPS1	0.1281	117.18
N2	20.9856	271.16
M2	42.3485	211.63
S2	31.479	230.52
ETA2	6.4042	155.31
MO3	0.5542	144.63
M3	1.6709	241.05
MK3	0.5032	297.42
SK3	0.4863	55
MN4	0.4862	54.34
M4	0.1784	170.36
MS4	0.1466	218.79
S4	0.6856	336.7
2MK5	1.2122	251.51
2SK5	0.2478	62.86
2MN6	0.2751	93.08
M6	0.8521	231.34
2MS6	1.3081	274.4
2SM6	0.1776	337.56
3MK7	0.2055	80.07
M8	0.3418	299.14

general, the calculated flow pattern of the WTDC scenario (for three wind designs) is still similar to those of the TDC scenario, which means the tidal current is dominant for the flow pattern in the study area. However, the tidal flow pattern in the study area significantly happens for the small scale (local effect). Overall, the flow pattern of the Malacca Strait shows the water moves to the northwest for the whole year (Devlin et al. 2018; Muhaimin et al. 2011; Wyrтки 1961).

## CONCLUSIONS

The present study suggests that the effect of tidal mixing is stronger than the effect of fresh-water discharge in controlling the coastal water properties in the study area, even though the measurement at the study site coincides with

**Table 5.** Tidal current ellipse components as recorded by a current meter

Tidal constituent	Major ellipse (m/s)	Minor ellipse (m/s)	Inclination (degree from east)	Phase (° GMT)
MSF	0.019	-0.011	125.59	187.37
2Q1	0.005	0.002	133.06	255.53
Q1	0.02	0.001	126.09	222.75
O1	0.018	-0.007	116.62	249.86
NO1	0.007	0.002	119.1	244.75
K1	0.045	-0.015	82	284.64
J1	0.011	0.002	8.95	331.96
O1	0.008	-0.003	128.63	311.7
UPS1	0.012	0	133.73	29.63
N2	0.038	0.006	78.54	284.99
M2	0.256	0.042	95.79	325.42
S2	0.091	0.021	93.35	338.54
TA2	0.014	-0.004	125.64	262.49
MO3	0.013	0	122.41	271.77
M3	0.01	0.006	173.59	75.56
MK3	0.024	0	110.87	124.87
SK3	0.015	-0.003	138.56	161.13
MN4	0.009	0.008	77.97	4.1
M4	0.016	0.004	149.32	105.86
MS4	0.008	0.004	157.03	104.05
S4	0.006	-0.001	88.8	280.06
2MK5	0.007	-0.005	82.94	293.53
2SK5	0.004	0.002	36.41	3.3
2MN6	0.008	0.004	111.92	242.2
M6	0.006	0.004	106.17	227.68
2MS6	0.006	0.003	139.72	299.93
2SM6	0.004	-0.003	80.01	339.69
3MK7	0.005	-0.001	146.24	91.51
M8	0.005	0.001	5.82	321.83

an intense La Niña event. The tidal range in the study area can reach 200 cm, corresponding to the strong tidal mixing where the observations show the contribution of the tidal elevation signal to more than 70%. The complex tidal propagation due to the confluence of tidal propagation from the Andaman and South China Seas and the influence of complex topography cause large nonlinear effects, as seen in the nonlinear tidal constituents for tidal elevation and tidal current in the study area. The M2 constituent is dominant in general, where the nonlinear tides produce over-tides of M4, M6, and M8. The simulated WTDC and TDC scenarios result in a similar flow pattern in the study area. This is consistent with the observed ocean current data that provides the tidal current signal accounting for 77% of total ocean current signal.

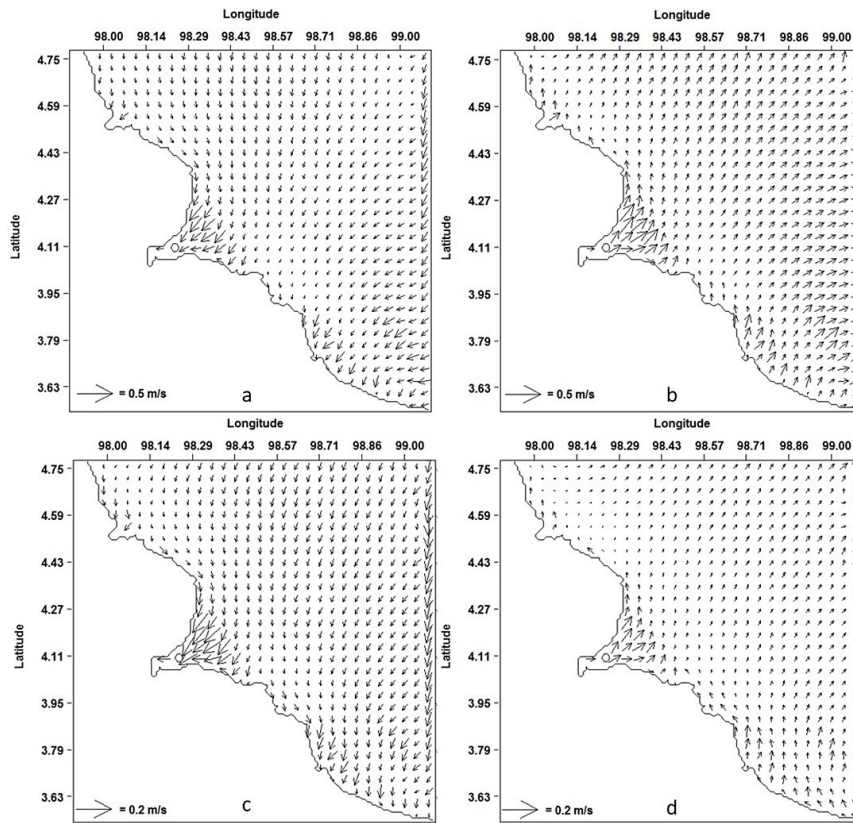


**Figure 6.** Model results for the TDC scenario during flood spring tide (a), ebb spring tide (b), flood neap tide (c), and ebb neap tide (d)

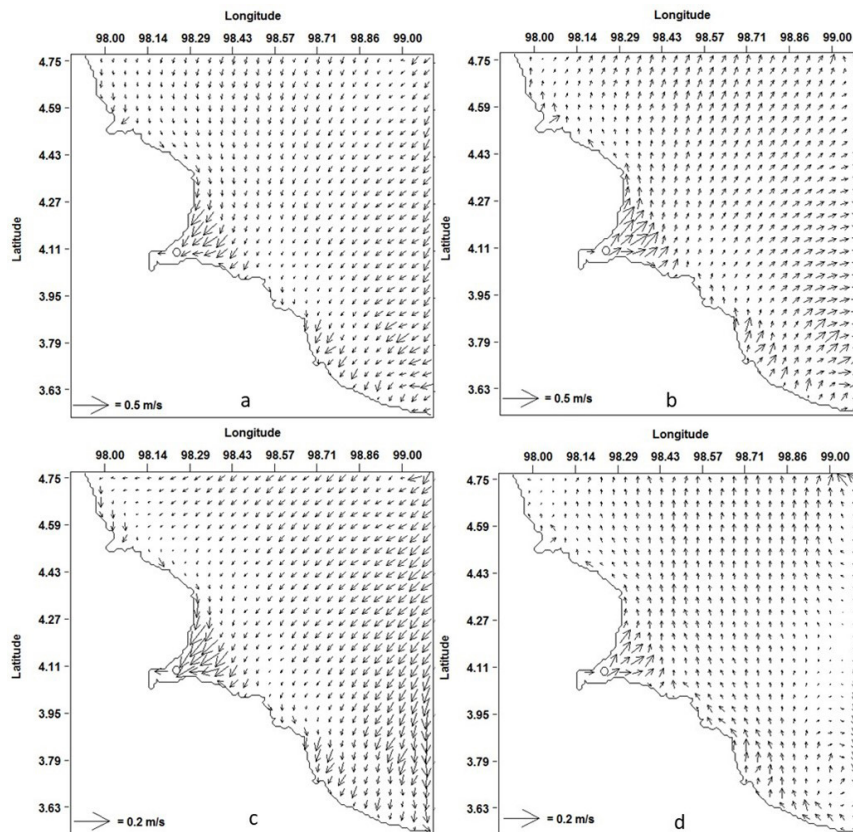


**Figure 7.** Model results for the WTDC-NE scenario during flood spring tide (a), ebb spring tide (b), flood neap tide (c), and ebb neap tide (d)

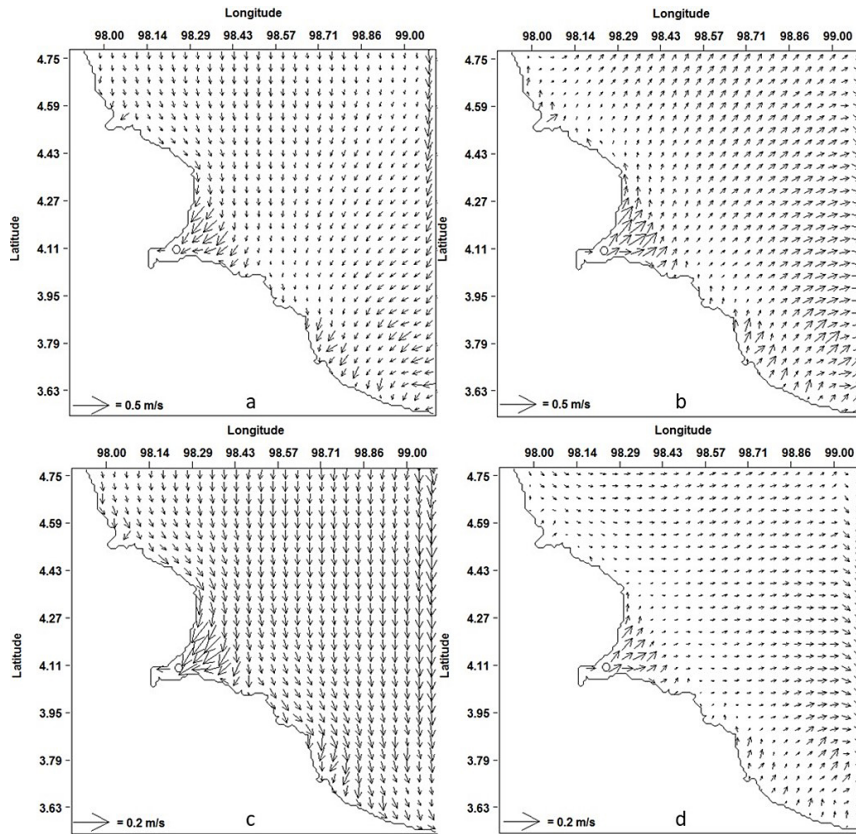


Figure 8. Model results for the WTDC-W scenario during flood spring tide (a), ebb spring tide (b), flood neap tide (c), and ebb neap tide (d)

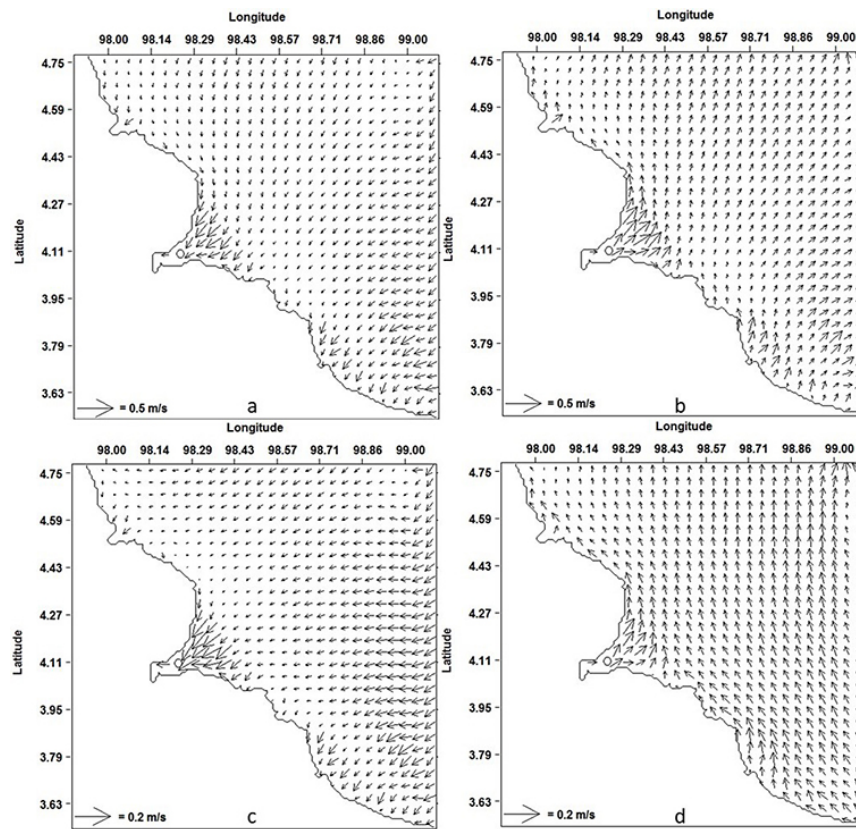


Figure 9. Model results for the WTDC-E scenario during flood spring tide (a), ebb spring tide (b), flood neap tide (c), and ebb neap tide (d)

## Acknowledgements

This study is supported by the Research Institute University of North Sumatra (Lembaga Penelitian Universitas Sumatera Utara).

## REFERENCES

1. Aldrian E., Dwi Susanto R. 2003. Identification of three dominant rainfall regions within Indonesia and their relationship to sea surface temperature. *International Journal of Climatology*, 23(12), 1435–1452.
2. Blumberg A.F., Ali Khan L., St. John J.P. 1999. Three-dimensional hydrodynamic model of New York harbor region. *Journal of Hydraulic Engineering*, 125(8), 799–816.
3. Blumberg A.F., Mellor G.L. 1987. A description of a three-dimensional coastal ocean circulation model. In: N. Heaps (Ed.) *Three-Dimensional Coastal Ocean Models*. American Geophysical Union, Washington, D.C., p. 1-16.
4. Chen H., Malanotte-Rizzoli P., Koh T.Y., Song G. 2014. The relative importance of the wind-driven and tidal circulations in Malacca Strait. *Continental Shelf Research*, 88, 92–102.
5. Chua T.E., Ross S.A., Yu H. 1997. Malacca Straits Environmental Profile. MPP-EAS Technical Report 10. Quezon City, Philippines.
6. Corrège T. 2006. Sea surface temperature and salinity reconstruction from coral geochemical tracers. *Palaeogeography, Palaeoclimatology, Palaeoecology*, 232(2–4), 408–428.
7. Daryabor F., Ooi S.H., Samah A.A., Akbari A. 2016. Dynamics of the water circulations in the Southern South China Sea and its seasonal transports. *PLoS ONE*, 11(7).
8. Deser C., Alexander M.A., Xie S.-P., Phillips A.S. 2010. Sea Surface Temperature Variability: Patterns and Mechanisms. *Annual Review of Marine Science*, 2(1), 115–143.
9. Devlin A.T., Zaron E.D., Jay D.A., Talke S.A., Pan J. 2018. Seasonality of tides in Southeast Asian waters. *Journal of Physical Oceanography*, 48(5), 1169–1190.
10. Durack P.J., Wijffels S.E. 2010. Fifty-Year trends in global ocean salinities and their relationship to broad-scale warming. *Journal of Climate*, 23(16), 4342–4362.
11. Fingas M. 2018. Remote sensing for marine management.” *World Seas: An Environmental Evaluation Volume III: Ecological Issues and Environmental Impacts*, 103–119.
12. Foreman M.G. 1977. Manual for Tidal Heights Analysis and Prediction. Pacific Marine Science Report Patricia Bay, Sidney, B.C., 77–10.
13. Foreman M.G.G. 1978. Manual for tidal currents analysis and prediction. Pacific Marine Science Report Patricia Bay, Sidney, B.C., 78–6.
14. Godin G. 1972. *The Analysis of Tides*. University of Toronto Press, Toronto, USA.
15. Haditiar Y., Putri M.R., Ismail N., Muchlisin Z.A., Ikhwan M., Rizal S. 2020. Numerical study of tides in the Malacca Strait with a 3-D model. *Heliyon*, 6(9), e04828.
16. Hii Y.S., Law A.T., Shazili N.A.M., Rashid M.K.A., Lokman H.M., Yusoff F.M., Ibrahim H.M. 2006. The strait of Malacca: Hydrological parameters, biological oxygen demand and total suspended solids. *Journal of Sustainability Science and Management*, 1, 1–14.
17. Ibrahim Z.Z., Yanagi T. 2006. The influence of the Andaman Sea and the South China Sea on water mass in the Malacca Strait. *Mer*, 43–44(4–1), 33–42.
18. Islam M.N., Maznah W.O.W. 2018. *Biomonitoring Ecosystem Health: Current State of Malaysian Coastal Waters*. Environmental Management of Marine Ecosystems, M. N. Islam and S. E. Jorgensen, eds., CRC Press, 287–305.
19. Jaya I., Siregar V., Sondita M.F., and Rustandi Y. 1998. *Marine and Coastal Resources Mapping for the Malacca Straits*. International Maritime Organization (IMO), Quezon City, Philippines.
20. Kowalik Z., Murty T.S. 1993. Numerical modeling of ocean dynamics. *Advanced Series on Ocean Engineering Volume 5*. World Scientific, Singapore – New Jersey – London – Hong Kong.
21. Mellor G.L. 2002. Users guide for a three-dimensional, primitive equation, numerical ocean model. *Ocean Modelling*, 8544(June), 0710.
22. Minhat F.I., Shaari H., Razak N.S.A., Satyanarayana B., Saelan W.N.W., Yusoff N.M., Husain M.L. 2020. Evaluating performance of foraminifera stress index as tropical-water monitoring tool in Strait of Malacca. *Ecological Indicators*, 111.
23. Muhaimin A.A., Zaiton Ibr Z., Aizat Isma S. 2011. Water Mass Characteristics in the Strait of Malacca using Ocean Data View. *Research Journal of Environmental Sciences*, 5(1), 49–58.
24. Osadchiev A., Medvedev I., Shchuka S., Kulikov M., Spivak E., Pisareva M., Semiletov I. 2020. Influence of estuarine tidal mixing on structure and spatial scales of large river plumes. *Ocean Science*, 16(4), 781–798.
25. Pang W.-C., Tkalich P. 2003. Modeling Tidal and Monsoon Driven Currents in the Singapore Strait. *Singapore Maritime and Port Journal*, 151–162.
26. Pawlowicz R., Beardsley B., Lentz S. 2002. Classical tidal harmonic analysis including error estimates in MATLAB using T\_TIDE. *Computers and Geosciences*, 28(8), 929–937.

27. Ramming H.G., Kowalik Z. 1980. Numerical Modelling of Marine Hydrodynamics. Elsevier Oceanography Series, Elsevier Science; 26.
28. Rusli M.H.B.M. 2012. Protecting vital sea lines of communication: A study of the proposed designation of the Straits of Malacca and Singapore as a particularly sensitive sea area. *Ocean and Coastal Management*, 57, 79–94.
29. Sangkoyo H., Adibroto T.A., Prionggo T., Setiawan D.R., Harahap D.N., Elfatih U., Faizal A. 2011. Pengembangan pusat keunggulan maritim – Selat Malaka menuju masyarakat berbasis pengetahuan. Penerbit Dewan Riset Nasional, Jakarta.
30. Sulbakti R. 2016. Analisis Spasial Potensi Banjir pada DAS Belawan dengan menggunakan Sistem Informasi Geografis (SIG). Universitas Sumatera Utara.
31. Susanto R.D., Pan J., Devlin A.T. 2019. Tidal mixing signatures in the Hong Kong coastal waters from satellite-derived sea surface temperature. *Remote Sensing*, 11(1).
32. Tan C.K., Ishizaka J., Matsumura S., Yusoff F.M., Mohamed M.I.H. 2006. Seasonal variability of SeaWiFS chlorophyll a in the Malacca Straits in relation to Asian monsoon. *Continental Shelf Research*, 25(2), 168–178.
33. Thia-Eng C., Gorre I.R.L., Adrian Ross S., Bernad S. R., Gervacio B., Corazon Ebarvia M. 2000. The Malacca Straits. *Marine Pollution Bulletin*, 41(1–6), 160–178.
34. Tomczak M., Godfrey J.S. 1994. Regional oceanography: an introduction. *Regional oceanography: an introduction*, Daya Publishing House, New Delhi, India.
35. Wu T., Wu H. 2018. Tidal Mixing Sustains a Bottom-Trapped River Plume and Buoyant Coastal Current on an Energetic Continental Shelf. *Journal of Geophysical Research: Oceans*, 123(11), 8026–8051.
36. Wyrтки K. 1961. *Physical Oceanography of Southeast Asian Waters*. University of California, Scripps Institution of Oceanography, La Jolla, CA.
37. Zhang H., Madsen O.S., Sannasiraj S.A., Soon Chan E. 2004. Hydrodynamic model with wave-current interaction in coastal regions. *Estuarine, Coastal and Shelf Science*, 61(2), 317–324.